THE JOURNAL OF PHYSICAL CHEMISTRY B

Article

pubs.acs.org/JPCB

Photoinduced Energy Transfer in Bichromophoric Pyrene–PPV Oligomer Systems: The Role of Flexible Donor–Acceptor Bridges

William Rodríguez-Córdoba,[†] Cesar A. Sierra,[§] Cristian Ochoa Puentes,[§] Paul M. Lahti,[‡] and Jorge Peon*,[†]

[†]Universidad Nacional Autónoma de México, Instituto de Química, Ciudad Universitaria, 04510, México, D.F., México

[‡]Department of Chemistry, University of Massachusetts, Amherst, Massachusetts 01003, United States

[§]Universidad Nacional de Colombia, Departamento de Química, Bogotá AA 14490, Colombia

Supporting Information

ABSTRACT: In this contribution, we report on the electronic energy transfer dynamics of bichromophoric systems incorporating two pyrene chromophores tethered by variable-length flexible alkyloxy chains to *p*-phenylenevinylene oligomers. These were studied using UV–vis absorption and both steady state and time-resolved fluorescence spectroscopy. Time-resolved emission measurements showed an efficient photoinduced energy transfer process in all the multichromophoric systems, which occurs on the time scale of tens of picoseconds after excitation at 265 nm. The energy transfer process is especially efficient in systems where the linker is formed by eight atoms (up to $k_{ET} \approx 2.7 \times 10^{10}$ s^{-1}), which, despite not being the shortest bridge studied, allows the approach of the donor and acceptor chromophores due to an appropriate number of flexible single bonds. Using Förster theory, we calculated the donor–acceptor distance in each triad from the experimental energy transfer rate, finding them to be in the range 8.8–10 Å.

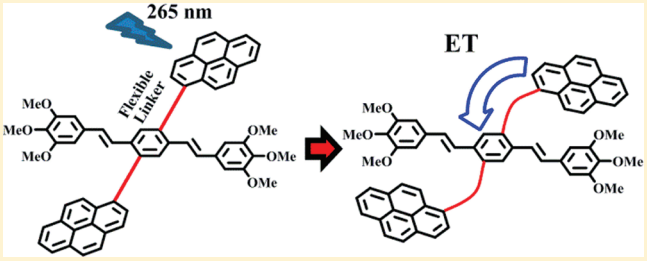

INTRODUCTION

The photosynthesis reaction sequence in nature has been the inspiration for the development of a large number of multichromophoric systems where the main objective has been the conversion of light into chemical energy or electricity.[1−6] Despite significant research on photoinduced energy and electron transfer processes in multichromophore compounds,[7−10] the design of new antenna–bridge–antenna systems, where the photon energy can be efficiently localized, remains the subject of extensive investigation.[2,7,8,10,11] Nowadays, the incorporation of polyaromatic chromophores to *p*-phenylenevinylene (PPV)[9] using different linker lengths has become an important challenge at the synthetic level, since the pendant groups must possess specific characteristics allowing the control of photophysical and solubility properties in different organic solvents.[12−17]

During the last two decades, a number of experimental time-resolved techniques and theoretical studies have focused on the characterization of electronic excited state properties and photophysical processes in several derivatives of *p*-phenylenevinylene oligomers.[18−25] The main difficulty in the study of these processes for PPV oligomers is that their complex decay behavior, which is similar to that of PPV polymers,[26−30] can involve several photophysical relaxation processes whose time scales reflect the natural structural fluctuations of the core structure. For example, Di Paolo et al.[23] reported that the fluorescent state of 2,5-di-[(2′-ethylhexyl)-oxy- and 2,5-di-[(3′-methylbutyl)-oxy]-*p*-phenylenevinylene trimers in solution shows triple exponential decays. In that work, the longest decay times (nanoseconds) were assigned to the lifetime of the trimer S_1 state, the shortest decay times (time scale of tens of picoseconds) were assigned to conformational relaxation processes, while intermediate times of hundreds of picoseconds were interpreted as the residual emission of *cis* isomer units. Therefore, all these processes need to be characterized and considered in the description of energy transfer processes which involve this core.

Several organic compounds with well-known photophysical properties have been used as light receptors in the synthesis of new multichromophore oligomers derived from PPV. In this contribution, we consider the use of pyrene moieties as auxiliary chromophores to indirectly excite these systems. The most important features of pyrene are its wide range of chemical reactivity, which allows a large number of structural modifications, its high molar absorption coefficient in the UV, and the large overlap between its fluorescence emission spectrum as a donor with the absorption spectra of several organic chromophores that can be used as acceptors. Pyrene is a highly symmetrical compound (D_{2h}), whose first two electronically excited states have been assigned with symmetry $^1B_{2u}$ and $^1B_{1u}$, respectively.[31,32] The electronic absorption spectrum of

Received: September 6, 2011
Revised: January 26, 2012
Published: February 22, 2012

pyrene in solution is primarily in the ultraviolet spectral zone (225−350 nm) with five intense and sharp bands. These spectral features allow the selective excitation of this polyaromatic ring when it is used as an antenna in different donor−acceptor systems. Although the first transition ($S_0 \rightarrow S_1$) is not forbidden by symmetry, it has a small extinction coefficient; however, it is nowadays accepted that, after a few picoseconds of the photoabsorption of short wavelength pulses, only the S_1 excited state is likely to be populated due to ultrafast internal conversion.[31,33] The fluorescence lifetime of pyrene in solution is up to hundreds of nanoseconds in different deoxygenated organic solvents (e.g., 374 ns in acetonitrile solution) and a few tens of nanoseconds in air-exposed solutions.[34−36] Such long excited-state lifetimes of pyrene in different media allow its use in efficient nonradiative relaxation processes as energy and electron transfer.

A steady state study of the energy transfer from the pyrene moiety to the short *oligo*-phenylenevinylene core in the systems used in this work—formed by PPV trimers bonded to pyrenic donors through flexible linkers (see Figure 1)—was previously reported by Sierra et al.[4] Specifically, the energy transfer quantum yield, Φ_{ET}, for each system was estimated by comparing

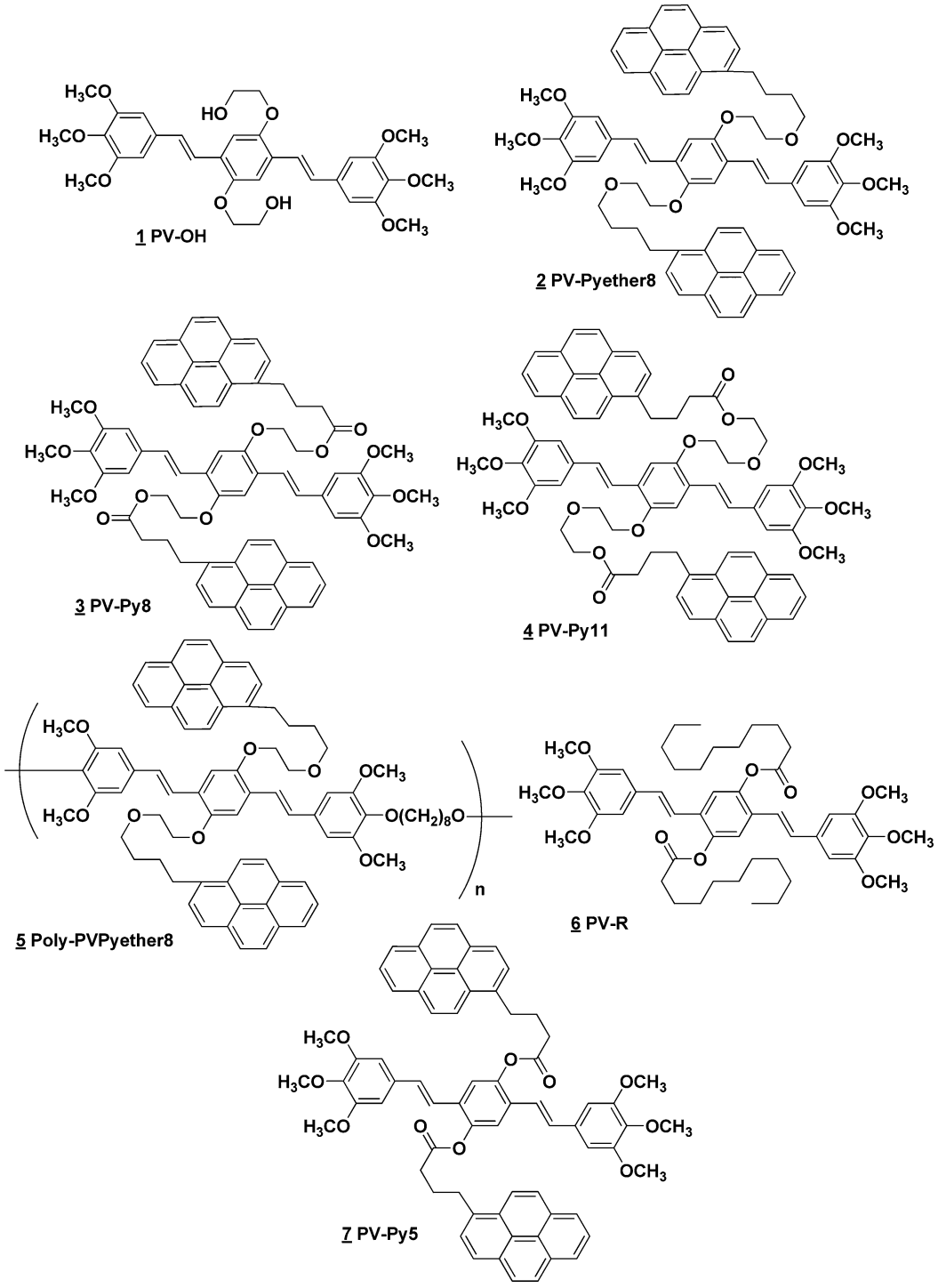

Figure 1. Molecular structures of the PPV derivative compounds used in this study.

dx.doi.org/10.1021/jp208602q | *J. Phys. Chem. B* 2012, 116, 3490−3503

absorption and excitation spectra following the procedure reported by Moore et al.[37] In the study by Sierra et al., the authors also reported that, after excitation of the pyrene donors at 276 nm, the steady state energy transfer efficiencies could be enhanced considerably depending on the nature and length of the linker. The optimal system found in the study by Sierra et al., with an energy transfer efficiency of 92% (solvent: chloroform), was an oligomer linked to pyrene by a nonconjugated tether length of eight atoms.

Knowledge of the actual energy transfer time scales in these systems requires a complete time-resolved spectroscopy investigation. This can clarify, among other things, if the transfer process occurs instantaneously from prearranged conformations or if the transfer rates are more consistent with donor−acceptor (D−A) lengths of somewhat more extended conformations. The direct measurement of the transfer rate can also clarify the kind of transfer mechanism responsible for the energy transfer events. The present measurements also allow for a direct comparison of the different molecular time scales, including electronic dynamics within the initially excited pyrene section, vibrational and orientational relaxation, and finally PPV and pyrene excited state decays.

Overall, we studied the photophysics of compounds **1**−**7**, focusing on fluorescence up-conversion studies of the photoinduced energy transfer process in four *p*-phenylenevinylene (PPV) oligomers **2**−**4** and **7**, plus one segmented *p*-phenylenevinylene copolymer, **5**, where each compound has two appended pyrene units linked by the flexible alkyl chains shown in Figure 1. Comparisons were made with the reference compounds that do not incorporate pyrene units. The understanding of their overall photophysical properties is of interest in the design and development of new photonic materials.[38−45] Due to the different absorption and emission features of the chromophores in the triads, we elucidated separately the excited state decays of *p*-phenylenevinylene reference compounds (**1** and **6**) along with all the multichromophoric systems, using selective excitation pulses tuned where one of the components is the primary absorbing unit. In this study, we also include several molecular modeling calculations which are valuable for comparing the experimentally determined D−A distances with the distances that correspond to different molecular conformations.

Our results showed that the time scale for the photoinduced energy transfer process is governed by molecular fluctuations and rotations, which take place on a much shorter time scale relative to the fluorescence lifetime of pyrene and PPV. Most importantly, our results demonstrate that the length of the linker has quite a strong effect on the energy transfer rates.

EXPERIMENTAL METHODS

Materials. The structures from Figure 1 used in this study consist of five multichromophoric pyrene−PPV oligomers tethered by flexible alkyloxy chains with well-ordered chemical structures (compounds **2**−**5** and **7**) and two alkyloxy-*p*-phenylenevinylene oligomers (compounds **1** and **6**) used as reference compounds. Full details of the synthetic methodologies and characterization of the model compounds **1**−**7** have been reported elsewhere.[4]

Time-Resolved Experiments. The fluorescence up-conversion spectrometer used in these experiments is based on a regeneratively amplified Ti:sapphire laser system (Coherent Legend, ∼800 nm, 150 fs, 1 kHz repetition rate) pumped by a Q-switched Nd:YAG (Clark-ORC-1000, 532 nm, 1 kHz repetition rate) and seeded with the output of a mode-locked Ti:sapphire oscillator (Clark-MXR, NJA-5) pumped by a Verdi V5 laser (Coherent Inc., 527 nm). The ∼800 nm output beam from the regenerative amplifier was split into two parts with a 1% beam splitter. The reflected pulse was used as a gate pulse, and coursed through an optical delay line and a half wave plate to adjust its polarization to the vertical direction. The transmitted fundamental beam was split again into two beams with a 50% beam splitter. One part was used to generate the second harmonic (400 nm) in a 0.5 mm β-barium borate (BBO) type-I crystal. The other part of the 800 nm pulse was adjusted to be vertically polarized with a half-wave plate and directed to an optical delay which allows the timing of the two pulses to be coincident by changing the path length. The two beams were collinearly recombined in a second 0.5 mm BBO type-I crystal to generate the third harmonic (∼265 nm). The third harmonic pulses were then passed through a CaF_2 prism compressor, sent through a zero-order half wave plate, and focused into a 1 mm path length flow cell containing the sample. The wave plate allowed for adjustment of the polarization of the excitation beam so that magic-angle, parallel, or perpendicular components of the fluorescence may be detected (in the setup, the lab-frame emission detection axis is fixed; see below). After the sample, the fluorescence emission was collected with two off-axis parabolic mirrors and focused onto a 0.5 mm BBO type-I crystal. The up-conversion signal was obtained by sum-frequency generation with the vertically polarized fundamental pulses (idler field) in a noncollinear configuration. The extraordinary crystal axis corresponded to the horizontal direction so that the vertical component of the emission (signal field) is detected. The resulting signal was focused to a double monochromator (Oriel) and detected with a photomultiplier tube connected to a lock-in amplifier (Stanford SR830) referenced to a 333 Hz phase locked optical chopper in the path of the pump beam. The instrumental response functions (IRFs) can be well represented by a Gaussian function with a fwhm of 590 ± 50 fs (225 ± 30 fs in the time-resolved experiments using second harmonic excitation pulses), and were determined through a cross-correlation scheme between the gate pulses and the Raman scattering of the pump beam in acetonitrile. The time-resolved emission anisotropy $r(t)$ was calculated directly from the use of excitation pulses with parallel or perpendicular polarizations with respect to the (fixed) vertical detection axis. Since only the excitation light polarization is rotated, it was unnecessary to use factors to scale the parallel and perpendicular polarized traces. All experiments were performed at room temperature. The femtosecond fluorescence time-resolved measurements, using excitation pulses of 410 nm, were performed similarly with the second harmonic beam generated directly in a 0.5 mm BBO crystal (type I phase matching) from the femtosecond pulse train of the Ti:sapphire oscillator (820 nm). Again, a waveplate was used to adjust the excitation pulse polarization. A detailed description of this system has been published previously.[46]

The kinetic traces were modeled as multiexponential decays analytically convoluted with the instrument response function. Time-resolved emission decays were measured at concentrations in the range 10^{-5}−10^{-6} M for the triads to obtain absorbance values less than 1 in all the absorption spectra. The influence of the concentration was checked in the range 3.0×10^{-7} to 6.0×10^{-5} M for all systems, and no changes in the shape of the stationary absorption spectra were observed. The acetonitrile solutions under study were frequently renewed and checked to verify the absence of photodegradation through steady-state spectroscopic measurements.

Steady State Spectroscopy. Electronic absorption spectra were recorded on a Cary-50 UV−vis spectrophotometer in a 1 cm quartz cell. The fluorescence emission and excitation spectra were recorded on a Cary Eclipse fluorimeter (Varian). The excitation spectra were corrected for the wavelength response of the system. The fluorescence quantum yields were obtained using Coumarin 343 (Aldrich, >99.5% purity) in ethanol as a reference, using an excitation wavelength of 390 nm.[47] All measurements were performed at room temperature in high purity liquid chromatography quality acetonitrile (Aldrich).

Computational Methodology. Molecular mechanics calculations using the MM+,[48] AMBER,[49,50] and BIO+[51,52] force fields were performed with the Hyperchem 8 software,[53] while UFF[54] force field computations were implemented with Gaussian 09.[55] For comparison purposes, the ground state geometries of the triads alone were also locally optimized using density functional theory (DFT) with the B3LYP[56] functional using a 3-21G* basis set. For all the triads under study, to establish minimum energy conformations in the ground state, a conformational search, varying all the dihedral angles of the linkers and the PPV core, was performed using the conformational search model of Hyperchem with the MM+ force field. For each compound, minimum energy conformers from MM+ were used as the starting geometry for DFT and molecular mechanics calculations. All frequencies were calculated at each methodology to verify the absence of negative frequencies that distinguish stationary states from saddle points.[53,55]

RESULTS

The steady state absorption spectra of acetonitrile solutions of multichromophores **2**−**5** and **7** compared with those of their respective reference oligo-PV model molecules with pendant alkyl arms (**1** and **6**) are shown in Figure 2. The

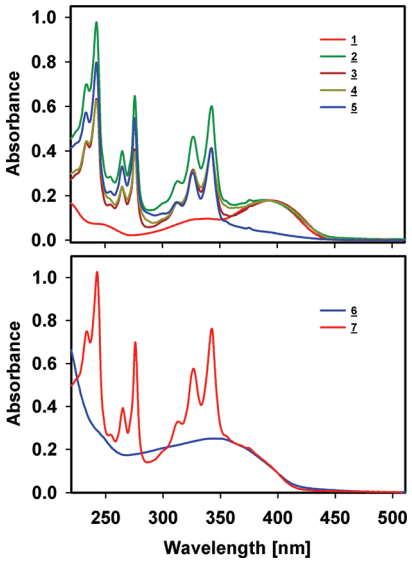

Figure 2. Absorption spectra of compounds **1**−**7** in acetonitrile solution.

absorption spectra of the multichromophore systems in solution look like overlays of the spectra of pyrene and the model oligo-PV molecules with two distinct absorption regions. The spectral zone below 350 nm shows the characteristic pyrenic peaks at approximately 245, 269, 279, 315, 330, and 346 nm. On the other hand, the broad band observed at 350−450 nm corresponds to the $S_0 \rightarrow S_1$ electronic transition (π−π^*) of the functionalized *p*-distyrylbenzene unit.[20,57,58] For compounds **2**−**5**, the first PPV type transition presents a maximum around 390 nm, while system **7** exhibits a blue-shifted core absorption band similar to PV-R oligomer **6**. Additionally, comparing the absorption spectra of the triads according to their linker lengths, the absorption bands below 350 nm (due to the pyrene chromophores) do not change significantly by changing the tether length from 5 to 11 atoms or when the functional group is changed from ether to ester. Similarly, the bands above 350 nm due to the PPV chromophores do not change in either peak position or spectral shape for the copolymer and triads with 8 and 11 linker lengths. However, this band does show some change when the linker length is five atoms because of having an ester unit attached directly to the PPV core. The different absorption patterns of compound **7** PV-Py5, which is the multichromophoric system with the shortest linker length, were explained by Sierra et al.[4] in terms of PPV core perturbation due to the presence of attaching a conjugating carbonyl group directly to the core chromophore.

The emission spectra of acetonitrile solutions were recorded at different excitation wavelengths (Figure 3). All the multichromophore compounds show emissions which are dominated by the central core. The emission spectra of **2**, **4**, and **7** show only small amounts of fluorescence from the pyrene moiety between 350 and 400 nm, while compound **5** shows a more prominent pyrenic emission. On the other hand, the fluorescence of compound **3** practically does not present any detectable emission of the pyrene moiety, even when the system is directly excited at a wavelength where the pyrenic electronic transitions dominate the absorption spectrum. The emission bands of compounds **2**−**5** present a maximum at about 445 nm with shoulders around 465 nm. The similarity in the emission spectra for all the multichromophore triads in this group relative to reference compound **1** (dotted line in Figure 3) is remarkable, with only minor variations in the spectra as functions of the pendant tethering group length of the tether. Similarly, the fluorescence emission spectrum of triad **7** is strikingly similar to that for oligomer **6** (dashed line). This result confirms that the different absorption and emission behavior of **7** is caused by the direct junction of the ester functional group to the PPV core, producing an electronic interaction that affects the ground and excited states of the core.

The large Stokes shift displayed in the absorption-emission spectra of the model compounds is a common feature of systems with significant differences in geometry between their ground and relaxed first excited states. These results show that the enhanced or virtually exclusive emission from the multichromophore PPV cores at approximately 445 nm upon excitation in the spectral range 265−330 nm, where pyrene is the main absorber, is due to photoinduced energy transfer from the excited pyrene chromophore to the PPV acceptor core. Summaries of the absorption, excitation, and emission spectra and the Stokes shifts observed in the model compounds in acetonitrile solutions are included in the Supporting Information. The fluorescence quantum yields (QY) in acetonitrile are also given in the Supporting Information (Table S4): all the compounds show significant emission strength and QY that are consistent with the QY previously reported[6] for less polar solvents.

Figure 4 shows frequency up-conversion measurements for compounds **1**−**7** in acetonitrile solution. These figures correspond to experiments exciting the PPV core directly at 410 nm and detecting the fluorescence emission at 485 nm. For all the PPV derivatives, the emission decays fit best to a

dx.doi.org/10.1021/jp208602q | J. Phys. Chem. B 2012, 116, 3490−3503

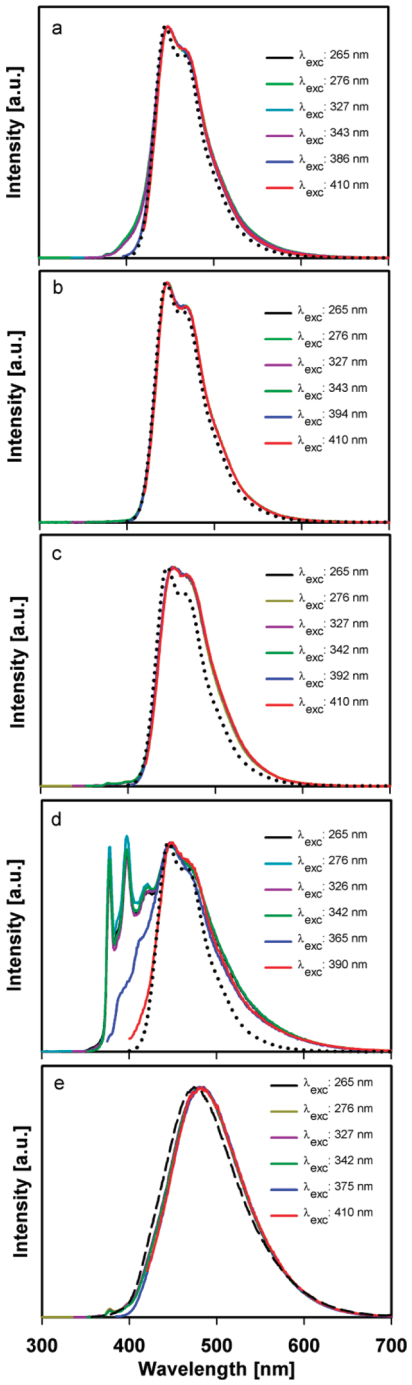

Figure 3. Emission spectra of the triads **2** (a), **3** (b), **4** (c), **5** (d), and **7** (e) (solid lines) and comparison with the reference compounds **1** (dotted line) and **6** (dashed line) in acetonitrile solution. The emission spectra of the triads were recorded using different excitation wavelengths in the spectral range 265–410 nm. Ordinates in each plot are scaled relative to one another for ease of comparison.

three-exponential function. The results of the multiexponential analysis are summarized in Table 1. For all systems, the fluorescence decay of the PPV core is dominated by a long decay time τ_1 with contributions up to 97% of the total decay and time constants between 1.1 and 1.4 ns.

As shown in Table 1, the values of the intermediate time constants τ_2 differ even when the linkers are the same length (as in compounds **2**, **3**, and **5**), and especially when the linker is directly attached to the *p*-phenylenevinylene core by different functional groups. The systems with ether functionalization give intermediate decay times between 30 and 90 ps with initial decays in the picosecond range (except for reference compound **1**). However, systems **6** and **7** with *ester* functionalization have τ_2 of less than 10 ps with initial decay on the femtosecond time scale. These results indicate that the fluorescence decay of the PPV cores does depend on the nature of the linker, such that even a small modification in the length, substitution pattern, or functionalization can modify the relaxation of the excited state. In subsequent discussion, these variations are put in context with energy transfer dynamics.

Once the emission decay profiles of the PPV core in the different oligomers were established, we studied the evolution of the fluorescence anisotropy in the multichromophoric systems in order to determine the time evolution of orientation of the excitation–emission transition dipole moments, and how the time scale for this process compares with time scales for energy transfer (see below). The emission anisotropy as a function of time was calculated according to the general equation $r(t) = (I_{\parallel} - I_{\perp})/(I_{\parallel} + 2{\cdot}I_{\perp})$ at 485 nm after excitation of the core with 410 nm pulses, and was evaluated directly from the up-conversion data taken with parallel ($I_{\parallel}$) and perpendicular ($I_{\perp}$) excitation-detection configurations.

The emission anisotropy was modeled with a biexponential function, except for segmented copolymer **5** where the signal was fit to a triexponential function. The results are summarized in Figure 5 and in Table 2. The anisotropy near $t = 0$ for all the model compounds is in the range of 0.31–0.37 (see continuous lines in the insets, see also Supporting Information), and the emission depolarization occurs in the tens to hundreds of picoseconds time scale (see Table 2). For molecules like the ones in this study, with considerably flexible linkers, the $r(t)$ decays represent the time scales in which the systems adopt multiple conformations and relative orientations of the donor–acceptor transition dipoles, with changing distances between the donor–bridge and acceptor sections.

In addition to the measurements on the triads, we studied the dynamics of the excited states of pyrene using the up-conversion technique in acetonitrile solution. Figure 6 shows traces for pyrene in acetonitrile solution in long and short time ranges, using excitation at 265 nm and fluorescence detection at 370 nm, near the onset of pyrene's S_1 emission. The trace is dominated by an ultrafast decay component of more than 88% amplitude in the multiexponential decay. This is consistent with emission from the upper singlet state that precedes formation of the first excited singlet S_1 having a larger oscillator strength for spontaneous emission to the ground state at the detection wavelength.[31−33] The data was modeled with a three-exponential decay analytically convoluted with the instrument response function: the longest time constant was unresolved due to its slow decay (see the Discussion section for a detailed explanation of the fitting procedure).[34]

By this analysis, we observed emission decays with time constants of $\tau_1 = 138 \pm 10$ fs and $\tau_2 = 1.47 \pm 0.5$ ps with pre-exponential factors of $\alpha_1 = 0.88$ and $\alpha_2 = 0.09$ and $\tau_3 \geq 20$ ns, respectively. The ultrafast fluorescence component in the femtosecond range corresponds to the $S_n \rightarrow S_1$ internal conversion process. The ~140 fs component should be taken as an upper limit due to our time resolution. To the best of our knowledge, this is the first report of the dynamics of the excited state of pyrene through the resolution of its spontaneous molecular emission. By comparison, in a recent report by Raytchev et al.[33] using the femtosecond time-resolved transient *absorption*

dx.doi.org/10.1021/jp208602q | J. Phys. Chem. B 2012, 116, 3490–3503

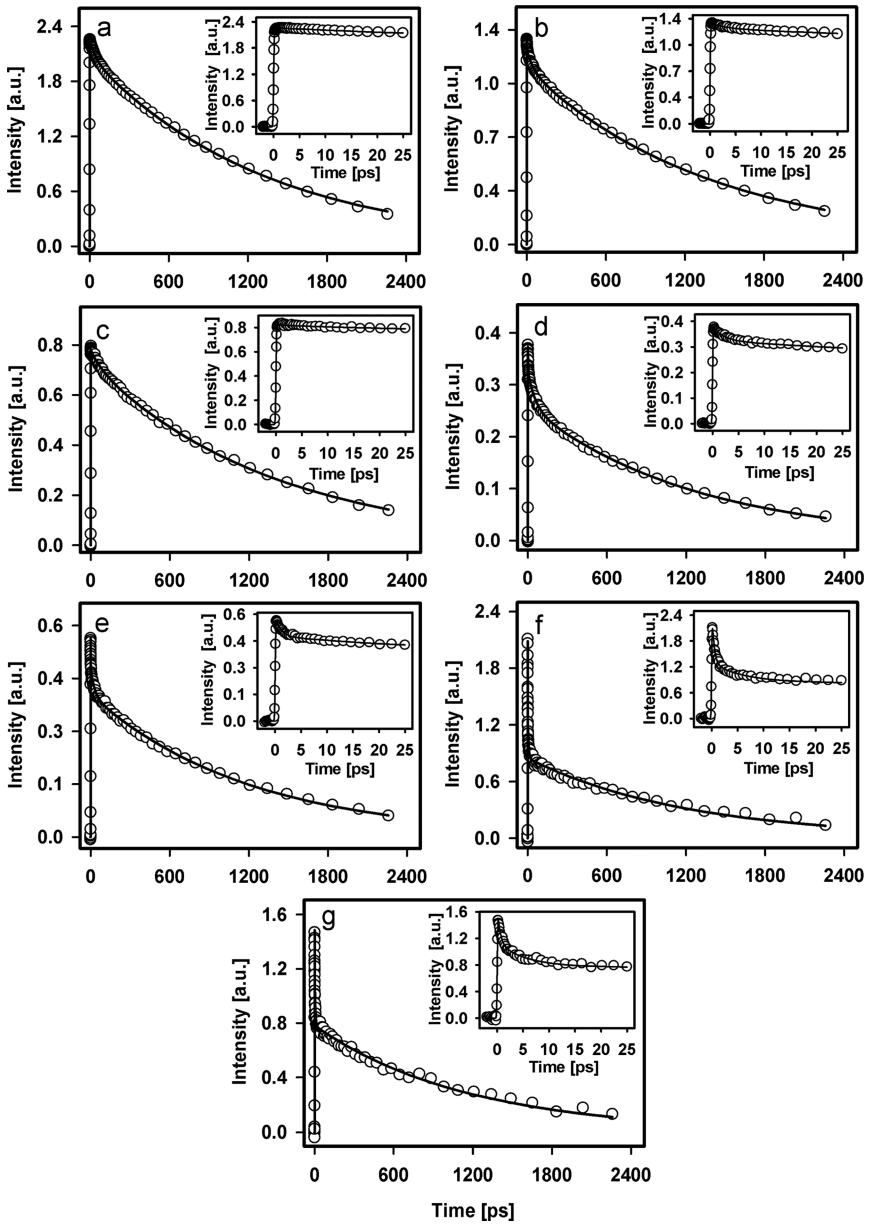

Figure 4. Femtosecond fluorescence up-conversion measurements of the multichromophores and related compounds in acetonitrile solution: (a) **1** (PV-OH), (b) **2** (PV-Pyether8), (c) **3** (PV-Py8), (d) **4** (PV-Py11), (e) **5** (Poly-PVPyether8), (f) **6** (PV-R), and (g) **7** (PV-Py5). Fluorescence and excitation wavelengths were 485 and 410 nm in all cases. Solid lines are convoluted multiexponential fits to the data. The insets show the fluorescence decays in the tens of picoseconds time range.

Table 1. Fluorescence Decay Times of Compounds 1−7 in Acetonitrile Solution Measured after Direct Excitation of the PPV Core at 410 nm and Detecting the Fluorescence Emission at 485 nm[a]

compound	α_1	α_2	α_3	τ_1 (ps)	τ_2 (ps)	τ_3 (ns)
1 PV-OH	−0.06	0.09	0.97	0.31 ± 0.09	44 ± 4	1.33 ± 0.04
2 PV-Pyether8	0.05	0.09	0.85	3.03 ± 0.09	50 ± 4	1.39 ± 0.05
3 PV-Py8	0.01	0.06	0.93	4.84 ± 0.15	88 ± 4	1.39 ± 0.04
4 PV-Py11	0.15	0.17	0.68	2.11 ± 0.18	55 ± 4	1.26 ± 0.04
5 Poly-PVPyether8	0.19	0.13	0.68	1.04 ± 0.12	29 ± 4	1.20 ± 0.05
6 PV-R	0.50	0.17	0.32	0.43 ± 0.06	6.1 ± 0.5	1.21 ± 0.47
7 PV-Py5	0.33	0.21	0.46	0.52 ± 0.09	5.3 ± 0.5	1.15 ± 0.04

[a]In all cases, the time-resolved emission curves were described by triple-exponential functions convoluted with the instrument response function. These figures correspond to experiments exciting directly the PPV core at 410 nm and detecting the fluorescence emission at 485 nm.

technique, the internal conversion process in pyrene occurs with a time constant of 78 and 89 fs in optical path lengths of 100 μm and 1 mm, respectively. The results from the present measurement established a time scale for the formation of the

dx.doi.org/10.1021/jp208602q | J. Phys. Chem. B 2012, 116, 3490−3503

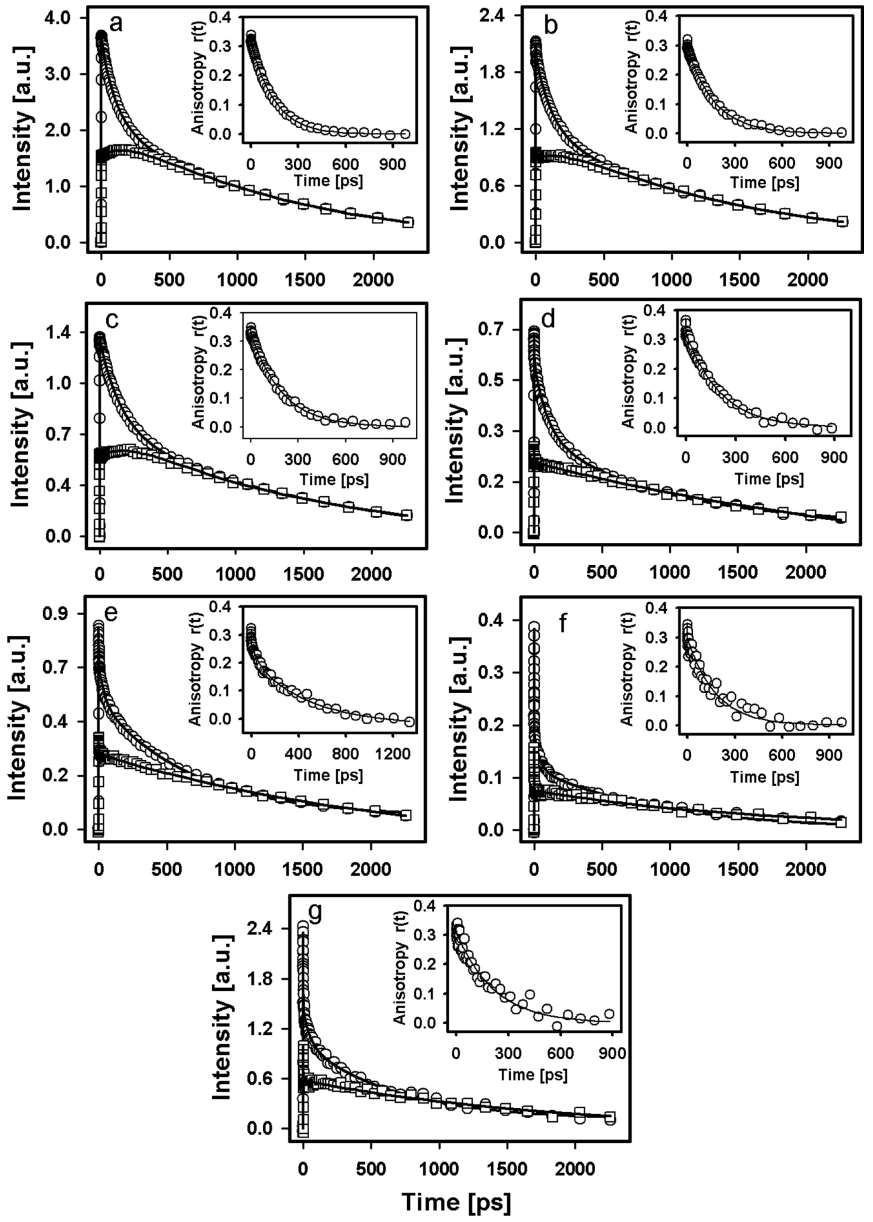

Figure 5. Main graphs: femtosecond fluorescence up-conversion measurements of the multichromophores and related compounds in acetonitrile solution taken with parallel (circles) and perpendicular (squares) excitation-detection configurations. (a) **1** (PV-OH), (b) **2** (PV-Pyether8), (c) **3** (PV-Py8), (d) **4** (PV-Py11), (e) **5** (Poly-PVPyether8), (f) **6** (PV-R), and (g) **7** (PV-Py5). In all cases, fluorescence and excitation wavelengths were 485 and 410 nm. Solid lines are convoluted multiexponential fits to the data. The insets show the anisotropy values calculated from the two experimental traces.

Table 2. Anisotropy Decay Times of Compounds 1−7[a]

compound	α_1	α_2	α_3	τ_1 (ps)	τ_2 (ps)	τ_3 (ps)
1 PV-OH	0.10	0.90		0.06 ± 0.01	147 ± 4	
2 PV-Pyether8	0.12	0.88		0.07 ± 0.02	172 ± 3	
3 PV-Py8	0.10	0.90		0.06 ± 0.02	197 ± 4	
4 PV-Py11	0.17	0.83		0.08 ± 0.02	208 ± 3	
5 Poly-PVPyether8	0.15	0.17	0.68	0.32 ± 0.03	55 ± 3	485 ± 6
6 PV-R	0.15	0.85		0.19 ± 0.02	178 ± 4	
7 PV-Py5	0.31	0.69		0.09 ± 0.02	216 ± 4	

[a]All samples were excited at 410 nm, and the fluorescence emission was detected at 485 nm.

pyrenic first singlet excited state upon excitation to an upper singlet (265 nm), a time scale that needs to be compared with the energy transfer times (see below).

The energy transfer measurements in the multichromophoric systems were made by specifically detecting the increase in PPV type emission after excitation near the pyrenic S_6 state at

dx.doi.org/10.1021/jp208602q | J. Phys. Chem. B 2012, 116, 3490−3503

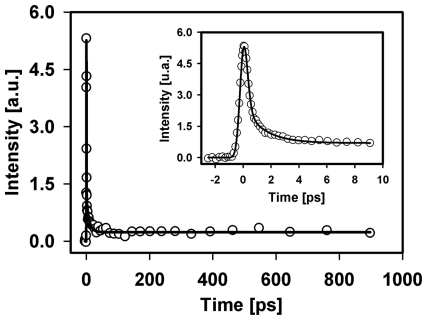

Figure 6. Fluorescence up-conversion measurements of pyrene in acetonitrile solution in the hundreds of picoseconds time range. The inset shows the ultrafast emission decay in the first picoseconds. The excitation wavelength was 265 nm, and the fluorescence was detected at 370 nm. The solid lines are nonlinear least-squares fits to triple exponential decays convoluted with the instrument response function.

265 nm. As expected, the fluorescence up-conversion curves of the triads show a rise time component when the emission of the PPV core is detected at its maximum emission wavelength. In Figure 7, we show the up-conversion traces for the triads in the time range of several hundreds of picoseconds (solid red lines). For descriptive purposes, these traces were modeled with triexponential functions and the results are summarized in Table 3. From these measurements, we found rising components (negative coefficients) with time constants up to several tens of picoseconds. The long decay times (t > 1 ns) practically correspond to the fluorescence lifetime of the relaxed PPV excited state (see the kinetic scheme for energy transfer, Scheme 1), and compare very well with the decay times obtained by direct excitation of the core with 410 nm pulses (see Table 1). Also, the emission decay of reference compounds **1** and **6** after excitation at 265 nm present the same decay profile as shown in Figure 4, and do *not* show a rise component. The first rise time components (τ_1) were assigned to vibrational relaxation processes from those molecules that are directly excited at the core (direct PPV absorbance at 265 nm is significant), while the second ones (τ_2) were assigned to the energy transfer process following pyrenic excitation. Overall, compound **2** is the only one that presents a first time constant over 10 ps (τ_1 = 16.6 ps). This will be clarified in the energy transfer discussion section.

In order to exclude the possibility that the first time constant component is due to energy transfer from a higher excited state of pyrene to the PPV acceptors, we measured the fluorescence decay of the pyrene unit at the short-wavelength side of its fluorescence spectrum (368 nm) after excitation with 265 nm pulses for compound **2**. The fluorescence up-conversion results are shown in Figure 8 in the long and short time scale. They show that emission from an upper pyrenic singlet state in the triad is characterized by an ultrafast component of 322 ± 10 fs, followed by a slower component of 2.2 ± 0.5 ps (typical of vibrational relaxation) with pre-exponential factors of α_1 = 0.83 and α_2 = 0.13, respectively. The results are similar to those discussed earlier for free pyrene, assigned to the $S_n \rightarrow S_1$ internal conversion process. After these two decay features, the signal shows a slower decay whose time constant cannot be accurately determined due to its very small amplitude at this wavelength.

To establish a direct assignment of the energy transfer time constants, we determined individual rate constants using the kinetic model of Scheme 1. Here, k_2 is the sum of the rate constants for radiative and nonradiative decay channels of the

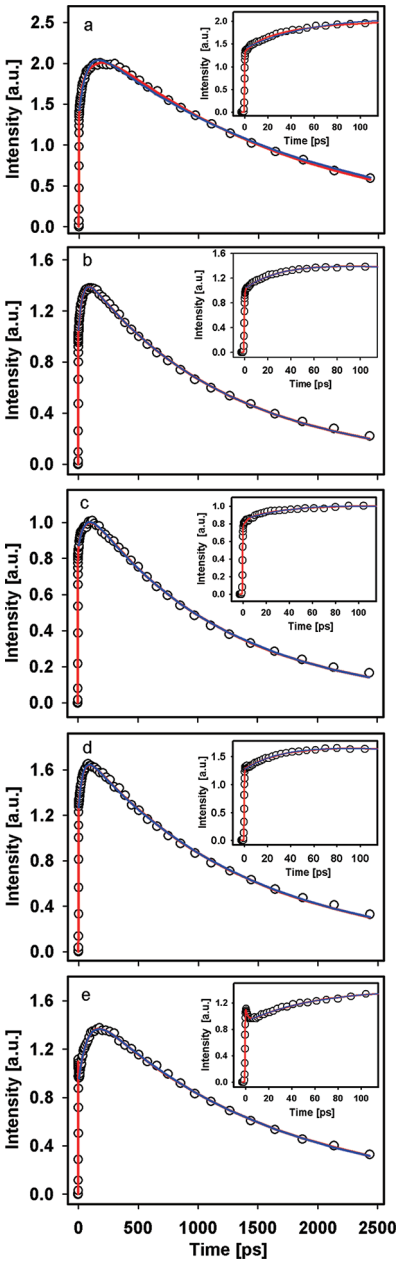

Figure 7. Femtosecond fluorescence up-conversion measurements of the triads in acetonitrile solution (red lines) and the fits obtained from the kinetic scheme using eq 1 (blue lines): (a) **2** (PV-Pyether8, λ_{fluor}: 447 nm), (b) **3** (PV-Py8, λ_{fluor}: 448 nm), (c) **4** (PV-Py11, λ_{fluor}: 448 nm), (d) **5** (Poly-PVPyether8, λ_{fluor}: 446 nm), and (e) **7** (PV-Py5, λ_{fluor}: 476 nm). In all cases, an excitation wavelength of 265 nm was used with the magic angle configuration. Solid lines are convoluted multiexponential fits to the data. The insets show the rise time in the tens of picoseconds scale.

locally excited state of pyrene *by paths other than energy transfer*. k_1 is the total rate constant of decay of the locally excited S_1 state of the core, and k_{ET} is the rate constant for the pyrene to core energy transfer process. Upon excitation of the pyrene moieties at 265 nm and $S_n \rightarrow S_1$ internal conversion, the locally excited S_1 state of pyrene can decay by channels k_2 or populate the locally excited state of the PPV by unidirectional energy transfer k_{ET}. This explains the rising components in the fluorescence decay of the triads upon exciting the pyrene chromophores.

dx.doi.org/10.1021/jp208602q | J. Phys. Chem. B 2012, 116, 3490–3503

Table 3. Multiexponential Decay Parameters Obtained for the Fluorescence Decay of oligo-PV Triads 2−5 and 7 in Acetonitrile Solution after Excitation with 265 nm Pulses[a]

compound	α_1	α_2	α_3	τ_1 (ps)	τ_2 (ps)	τ_3 (ns)
2 PV-PyEther8	−0.26	−0.57	1.83	16.6 ± 1.4	124 ± 5	1.69 ± 0.05
3 PV-Py8	−0.39	−0.70	2.09	0.54 ± 0.12	35.2 ± 1.8	1.19 ± 0.05
4 PV-Py11	−0.13	−0.38	1.50	3.8 ± 0.6	61.1 ± 2.2	1.16 ± 0.05
5 Poly-PVPyether8	−0.42	−0.58	2.00	0.14 ± 0.03	38.7 ± 2.2	1.36 ± 0.04
7 PV-Py5	0.23	−0.60	1.37	1.88 ± 0.18	76 ± 3	1.50 ± 0.04

[a]In all samples, the fluorescence was detected at the maxima of the respective emission band.

Scheme 1. Kinetic Scheme for the Energy Transfer Process from the First Singlet Excited State of Pyrene to the First Singlet Excited State of the PPV Core

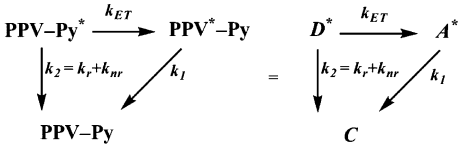

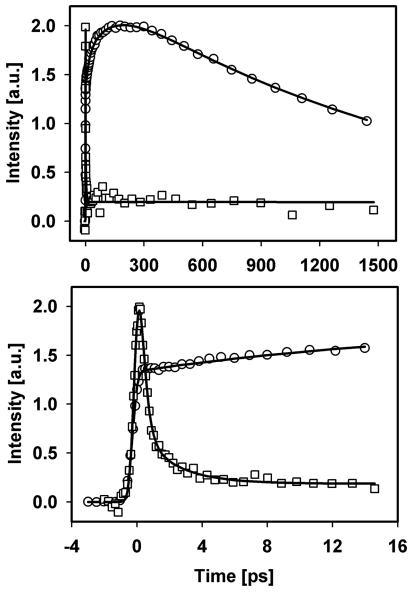

Figure 8. Comparison of the fluorescence up-conversion measurements of compound **2** in acetonitrile solution in the short- and long-time range. The excitation wavelength was 265 nm, and the fluorescence of the pyrene unit was detected at 368 nm (squares). The emission decay represented with circles corresponds to the emission of the PPV core detected at 447 nm. The traces have been scaled relative to one another for ease of comparison. The solid lines are nonlinear least-squares fits to a triple exponential decay convoluted with the instrument response function.

Taking into account that direct excitation of the acceptor (oligo-PV core) cannot be avoided when exciting the triads with 265 nm pulses, the concentration of excited acceptors following donor excitations is given by

$$[A^*]_{t'} = \left\{ \frac{k_{ET}[D^*]_0}{k_{ET} + k_2 - k_1} + [A^*]_0 \right\} e^{-k_1 t'} - \frac{k_{ET}[D^*]_0}{k_{ET} + k_2 - k_1} e^{-(k_{ET}+k_2)t'} \quad (1)$$

where $[A^*]_0$ is the concentration of directly excited acceptors at time $t = 0$. This equation is similar to one for typical sequential unimolecular reactions (I → II → III, where A* corresponds to intermediate species II) but where the precursor (D* corresponding to I) has an additional decay channel, which here arises from locally excited pyrene S_1 state decay channels other than energy transfer.

Figure 7 shows a comparison between the aforementioned convoluted multiexponential fits to the data (red solid lines) and the results obtained from the direct fits to data using eq 1 (blue solid line). As can be seen, the phenomenological rise times τ_2 (Table 4) indeed match reasonably well the time constants of the energy transfer processes by this model. For the case of compound **2**, the time constant associated with energy transfer ($1/k_{ET}$) appears to correspond to the average value between τ_1 and τ_2.

By using the experimentally obtained energy transfer rates, the energy transfer efficiencies were calculated using the general equation $\Phi_{ET} = k_{ET}/k_{ET} + k_2$. Table 4 lists the individual energy transfer rate constants and efficiencies for each system, based on the above analysis. The results show that energy transfer occurs in the tens of picoseconds time scale, somewhat shorter but similar to the diffusional rotation times of Table 3. Energy transfer is more efficient when the linker is formed by eight atoms, as in molecular triads **2** and **3** and in segmented copolymer **5**.

Energy Transfer Study to Establish a Förster Mechanism. Due to the ultrafast internal conversion process present in pyrene, after a few picoseconds only, its fully relaxed S_1 state is populated, regardless of the excitation energy. Thus, energy transfer in the pyrene−PPV triads occurs from the S_1 state of the pyrene donor to the S_1 state of the *oligo*-phenylene vinylene core (acceptor). The signal rises of Figure 7 establish that energy transfer occurs in the time scale of several tens of

Table 4. Individual Energy Transfer Rate Constants, Energy Transfer Efficiencies, and Decay Times Obtained from the Kinetic Model of Scheme 1 and eq 1

compound	k_2^{-1} [a] (ps)	τ_{ET} [a] (ps)	k_1^{-1} [a] (ns)	k_2 (s^{-1}) × 10^9	k_{ET} (s^{-1}) × 10^{10}	k_1 (s^{-1}) × 10^8	Φ_{ET}
2 PV-Pyether8	713 ± 4	74 ± 3	1.81 ± 0.04	1.40	1.34	5.53	91%
3 PV-Py8	917 ± 5	36 ± 4	1.19 ± 0.04	1.09	2.74	8.37	96%
4 PV-Py11	464 ± 3	63 ± 3	1.17 ± 0.04	2.16	1.58	8.57	88%
5 Poly-PVPyether8	479 ± 3	38 ± 4	1.37 ± 0.04	2.09	2.61	7.30	93%
7 PV-Py5	600 ± 4	88 ± 4	1.49 ± 0.04	1.67	1.13	6.69	87%

[a]τ_i and k_i were named relative to the kinetic model outline in Scheme 1.

dx.doi.org/10.1021/jp208602q | J. Phys. Chem. B 2012, 116, 3490−3503

picoseconds, comparable to that of the molecular reorientation processes probed in the experiements summarized by Figure 5 and Table 2. This is a singlet−singlet allowed transition, so the fact that modulation of the distance between the donor (pyrene) and the acceptor (PPV) influences the transfer dynamics suggests that energy transfer in these systems follows a Förster type mechanism.

According to Förster's theory,[59−62] the energy transfer rate between two chromophores can be calculated using the following equations

$$k_{ET} = k_D\left(\frac{R_0}{R}\right)^6 \quad (2)$$

and

$$k_D = (\tau_D)^{-1} \quad (3)$$

where τ_D is the excited singlet state lifetime of the donor in the absence of the acceptor, R is the distance between chromophores, and R_0 is the Förster critical transfer radius, defined as the distance between chromophores where the energy transfer process is 50% efficient. R_0 can be easily calculated from measurable spectroscopic quantities using eq 4

$$R_0 = \frac{9000 \ln 10 \Gamma^2 \Phi_D}{128\pi^5 n^4 N_A} J_{d-d} \quad (4)$$

where Γ^2 is an orientation factor, Φ_D is the quantum yield of donor in the absence of energy transfer, n is the refraction index of the solvent, and N_A is the Avogadro number. J_{d-d} is known as the spectral overlap integral for dipole−dipole interaction and is defined as

$$\int_0^\infty \frac{\overline{F}_D(\overline{\nu})\varepsilon_A(\overline{\nu})\, d\overline{\nu}}{\overline{\nu}^4} \quad (5)$$

where $F_D(\overline{\nu})$ is the fluorescence emission spectrum of the donor, $\varepsilon_A(\overline{\nu})$ is the absorption spectrum of the acceptor expressed by its extinction coefficient, and $\overline{\nu}$ is the average transition frequency in cm^{-1}. From our data, R_0 was calculated by eq 4 to be 40.8 Å, using $\Gamma^2 = 2/3$ assuming random orientation, $\Phi_D = 0.62$, $n_{ACN} = 1.344$, and $J_{d-d} = 4.16 \times 10^{-14}$ M^{-1} cm^3.

Finally, for every Py−PPV triad in this study, the donor−acceptor distance (R) was calculated using the experimentally obtained energy transfer rate. The results are summarized in Table 5.

Table 5. Individual Donor−Acceptor Distances (R) Calculated for the Pyrene−PPV Multichromophoric Systems Using the Förster Energy Transfer Theory

compound	donor−acceptor distance R (Å)
2 PV-Pyether8	9.9
3 PV-Py8	8.8
4 PV-Py11	9.6
5 Poly-PVPyether8	8.8
7 PV-Py5	10

Molecular Modeling Results. The donor to acceptor (PPV core) distances were modeled using the molecular mechanics force fields and DFT methodologies summarized in Table 6. Establishing reference points with regard to these distances was accomplished by comparing the observed Förster distances with pyrene to PPV distances at the "most-extended geometries" and with distances at local-minima conformations where the pyrene unit makes a close approach to the PPV core. The "most extended" geometries were established using force field methods to give the largest donor−acceptor distances (angles, distances, and dihedrals correspond to local minima of the force fields that give the longest pyrene to PPV distances). The "closest approach" geometries (second through last columns in Table 6) correspond to local or global minima in which the donor−acceptor distances are minimal. The observed donor−acceptor distances from Table 5 tend to fall intermediate between the most extended and closest approach geometries of Table 6, except for the system with the shortest linker, **7**, whose Forster radius is closest to the most extended model.

Table 6. Individual Center-to-Center Donor−Acceptor Distances (R) Calculated for the Pyrene−PPV Multichromophoric Systems Using Molecular Mechanics and DFT Methods[a]

	center-to-center donor−acceptor distance R (Å)					
		level of theory				
compound	extended geometry	MM+	AMBER	UFF	BIO+	B3LYP/ 321G*
2 PV-Pyether8	15.16	4.60	4.49	3.86	3.81	6.18
3 PV-Py8	15.17	4.04	4.09	4.48	3.78	5.77
4 PV-Py11	18.48	3.55	3.62	3.50	3.67	7.14
7 PV-Py5	11.30	4.75	4.25	5.15	4.32	7.46

[a]The extended geometries correspond to local minima where the combination of dihedral angles in the linkers gives the largest possible donor-to-acceptor distances. The rest of the columns indicate local minima at conformations where the pyrene−PPV distances are minimal for the respective methods.

DISCUSSION

Steady State Spectroscopy. Despite the similarities between the compounds used in this study, the steady-state absorption and emission spectra show differences relative to each other. For example (Figures 2 and 3), segmented copolymer **5** shows clear differences in its core absorption band relative to reference compound **1**. Comparing the structures of copolymer **5** (Poly-PVPyether8) with oligomer **2** (PV-Pyether8), there is no difference in the basic structure of the linker, antenna (pyrene), and *oligo*-phenylenevinylene core (Figure 1); the difference is in the octamethylene linkers between multichromophores moieties in **5**. One plausible explanation of the spectral differences in the PPV absorption band of these would be conformational and/or proximity effects for the multichromophores held together by nonconjugated octamethylene linkers in **5**.[4]

The emission and excitation steady state spectra of the reference and the triad compounds, acquired using different excitation and detection wavelengths, show that the structureless broad emission bands in the triads at about 450 nm correspond to the fluorescence emission of the PPV core *after* the photoinduced energy transfer process from the pyrene moiety. From the significant Stokes shift, we can conclude that the relaxed S_1 excited state geometry of the triads is somewhat different relative to the equilibrium ground state conformation.[63−69] Except for **5**, the emissions show minimal to negligible pyrene emissions, even when the systems are excited at the pyrenic bands in the UV. Copolymer **5** shows significant pyrene-type emission despite the fact that it shows one of the largest energy transfer rates and

dx.doi.org/10.1021/jp208602q | J. Phys. Chem. B 2012, 116, 3490−3503

efficiencies (93% from the time-resolved results). This can be trivially explained considering that the copolymer, which has an average length of 10 monomeric units, can form coiled structures in solution such that approach of the pendant pyrene donor to the PPV core is impeded. Such excited state geometries will give longer lived pyrenic excitations, with accumulation of steady state pyrene emission. The energy transfer efficiencies from the equation $\Phi_{ET} = k_{ET}/k_{ET} + k_2$ do *not* take into account this effect, which is exclusive to the polymer. The small (or negligible) amounts of pyrene emission from molecular triads are consistent with an approximately 90% or larger efficiency for energy transfer, where the most efficient system **3** (Table 4) shows no discernible pyrenic emission.

The absorption and excitation spectra of segmented copolymer **5** and reference compound **6** show differences indicating that the singlet−singlet energy transfer efficiency in these is not 100% efficient. This inhomogeneity in a polymeric structure, especially, would reasonably give populations of triad chromophores with reduced fluorescence and/or energy transfer capacity. Also, aggregates might occur in these cases. For example, Kozyra et al.[70] studied the 6-dodecanoyl-2-dimethylaminonaphthalene by steady-state and time-resolved fluorescence spectroscopy and explained the difference between the excitation and absorption spectra based on the formation of micelle aggregates. Similar to that molecule, PV-R **6** has two undecanoyl ester chains directly attached to the PPV core. Thus, **5** and **6** have possibilities for coiled structures or micelle complexes that could give the absorption-excitation spectral differences.[71] The (smaller) differences in the scaled excitation spectra with respect to the absorption spectra for the other systems can be ascribed directly to nonquantitative energy transfer.

Time-Resolved Florescence Emission of the oligo-Phenylenevinylene Core. Using the time-resolved up-conversion technique, we elucidated the emission decay of the *oligo*-phenylenevinylene core in the absence of the energy transfer process by exciting the triads at 410 nm, where the core is the sole absorber. None of the systems show emission from the pyrene moiety after photoexcitation of the PPV core around 350−450 nm (Figure S2 in the Supporting Information). Therefore, the time-resolved kinetics under these conditions correspond only to the evolution of the phenylenevinylene core excited states for each system (with the absence of the energy transfer process). Still, the results in Figure 4 show the core fluorescence decays to occur by multiple photophysical processes with different time scales during the relaxation of the excited state. The complex multiexponential decay profiles are analogous to the earlier-mentioned results reported by Di Paolo and Seixas de Melo for several *p*-phenylenevinylene trimers in different solvents.[22,23] We assigned the longest decay times, with a time scale of nanoseconds, to the fluorescence lifetimes of the systems, while the spectral evolution which takes place during the first picoseconds was ascribed to vibrational relaxation processes. For the case of the systems **1**−**4** and **7**, we assigned the intermediate decay times in the sub-100 ps time scales to conformational relaxation processes of the initially excited oligomer toward more planar conformations in the relaxed excited state. This interpretation has been supported by different experimental and theoretical studies performed in several aryloxy-*p*-phenylene and phenylene-ethylene oligomers.[63−69] However, for systems **5** and **6**, the assignment of the intermediate decay could be more complicated, as indicated by differences between absorption and excitation spectra, which suggests the coexistence of different conformers in the ground state. On the basis of this, the intermediate time constants can involve fluorescence emission contributions from multiple geometric species vibrationally evolving to equilibrium in the excited state.[71]

We now turn to the time-resolved anisotropy studies. With exception of copolymer **5**, which has an additional intermediate time constant in the tens of picoseconds time scale, the emission anisotropies of multichromophores show biexponential decay. As shown in Figure 5 and the Supporting Information, the $r(0)$ values range between 0.31 and 0.37 (see continuous lines in the Figure 5 insets). The emission anisotropy shows very fast relaxing components in the first 350 fs (insets in Figure S2, Supporting Information) with 10−31% contributions in the total anisotropy decay. After this modulation, of approximately 0.04 units, the emission anisotropy decays in the hundreds of picoseconds time scale. In several systems, rapid change in emission anisotropy has been attributed to solvent-induced mixing of different electronic levels and fast conformational changes within the fluorescent state.[72]

Such solvation dynamics, including both the inertial and the diffusive parts of the response, have been extensively studied by the group of Maroncelli. For acetonitrile, the spectral response function was fitted by a biexponential function with time constants of 0.089 and 0.63 ps.[73] These components were assigned to inertial motions of the solvent molecules and the solvent relaxation time, respectively. Contrary to the fast fluorescence depolarization components measured for the multichromophores in this study, the long time constants (ranging between 140 and 485 ps, Table 2) do not correspond to Maroncelli's solvent relaxation time of 0.63 ps for acetonitrile. On the basis of this, the long decays in Table 2 were assigned to rotational relaxation of excited state populations and the fast components (responsible for the ultrafast fluorescence depolarization) to solvation plus relaxation from torsional vibrations or inertial motions.

Most important, the intermediate time constants in the anisotropy decay quantify the time scale for molecular rotations, which are accompanied by exploration of several conformations about the flexible linker bonded to the donor site. The "drag" that the linker segments cause as the molecular core rotationally relaxes influences the average donor−acceptor distances and orientations. Interpreting the time scales of the energy transfer processes therefore requires caution in considering the role played by the flexible linkers.

Energy Transfer in the Multichromophoric Systems. The use of pyrene as an auxiliary chromophore in these multichromophores enhances their light-absorbing capacities in the ultraviolet, and more importantly promotes an efficient nonradiative energy transfer process after direct excitation with 265 nm light. Even though the fluorescence of pyrene in organic solvents can be strongly quenched by the presence of oxygen,[74] in aerated organic solvents, its lifetime remains in the tens of nanoseconds time scale, long enough to allow several nonradiative processes to compete directly with the fluorescence deactivation channel (e.g., nonradiative energy transfer). Time-resolved studies of pyrene in solution have demonstrated that relaxation of its higher excited states occurs on multiple time scales, with the first two component decays occurring from sub-100 fs to picoseconds.[31,33] As mentioned in the Results section, the fluorescence up-conversion decay of pyrene in acetonitrile solution was best modeled with a triexponential function with the longest time constant set to be more than 20 ns. Different fitting approaches were also tried, where the pyrene fluorescence

dx.doi.org/10.1021/jp208602q | J. Phys. Chem. B 2012, 116, 3490−3503

decay was fitted by a biexponential function plus a component with an infinite lifetime (as the fluorescence does not decay in our observation window), or with a triexponential function fixing the longest time constant to the corresponding fluorescence lifetime of pyrene in aerated acetonitrile of 18.6 ns.[35] This showed, as expected, that the experimental time constant τ_1 = 138 ± 10 fs (α_1 = 0.88) and τ_2 = 1.47 ± 0.5 ps (α_2 = 0.09) does not depend on the procedure used to fit the experimental data with regard to the long time decay component.

The time-resolved up-conversion measurement data presented in Figure 7 and Tables 3 and 4 show that the photoinduced energy transfer process efficiency follows a trend where the antenna (pyrene) is attached to the acceptor (PPV core) by linkers accordingly: k_{ET} 8 atoms > k_{ET} 11 atoms > k_{ET} 5 atoms. However, despite the differences of the linkers, the nonradiative energy transfer efficiency is remarkably high for all the multichromophore triads (87−96%). On the basis of the energy transfer efficiencies and rotational relaxation time constants, the energy transfer process is more influenced by molecular conformations and rotations than by linker length. This idea well fits the segmented copolymer **5** (with an Φ_{ET} = 93%) where, after direct photoexcitation of the pyrene antennae, a large fraction of the molecules can evolve rapidly into many different conformations while "finding" an optimal distance for the energy transfer from the antenna to the acceptor.

The general pathway of nonradiative energy transfer in the triads can thus be summarized as follows. Within a few femtoseconds of electronic excitation of the pyrene chromophore by 265 nm pulses, only its S_1 excited state remains populated. This process is governed by ultrafast $S_n \rightarrow S_1$ internal conversion in the ~300 fs time scale, as seen even in substituted pyrene derivatives.[33] The energy transfer process from the S_1 excited state pyrene antenna to the S_1 excited state core acceptor occurs on a time scale of tens of picoseconds. Since the rate for the pyrene's intrinsic de-excitation is much slower (several hundreds of picoseconds, see Table 4, k_2^{-1} values) than the energy transfer and conformational fluctuation processes (tens of picoseconds), the pyrene S_1 excited state of the triads evolves toward different conformations which modulate the donor−acceptor distance and orientation, and enhance the nonradiative energy transfer. The time scales representative of these fluctuations can be deduced from the anisotropy decay times (tens of picoseconds) of Table 2. Finally, after energy transfer, the core unit S_1 geometry relaxes to the ground state by fluorescence emission on a time scale of nanoseconds. The processes occurring upon excitation of the oligo-PV triads **2**−**5** and **7** in acetonitrile solution with either 410 or 265 nm light are depicted in the energy diagram in Scheme 2. All decay time values are assigned from experimentally observed results in the present study.

Expanding on the relation between molecular geometries and electron transfer rates, the "extended geometries" from Table 6 from the computations (1st column) give D−A distances that are approximately 50% longer than the experimental Förster distances. The observed *R* values of Table 5 are also significantly longer than the local minimum geometries with shortest D−A distances (columns 2−6 for the respective method in Table 6). The comparison of the experimental *R* values of Table 5 with the reference distances of Table 6 makes it clear that the D−A distances associated with the number of units in the linker in fully extended conformations are not the determining factor in the energy transfer process. The observed

Scheme 2. Energy Level Diagram of oligo-PV Triads 2−5 and 7 in Acetonitrile Showing Photophysics and Deactivation Pathways, upon Excitation (a) of the Pyrene at 265 nm and (b) of the oligo-PV Units at 410 nm

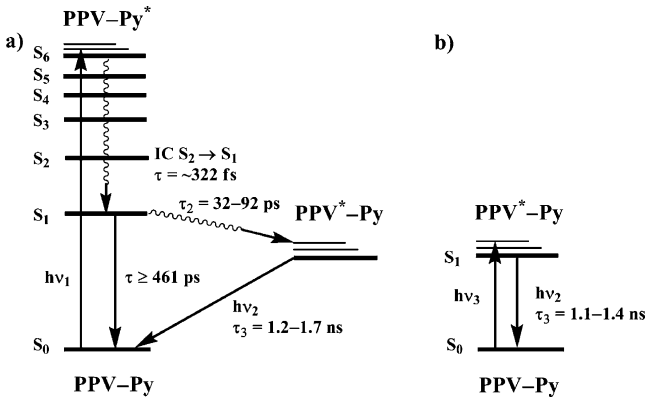

distances of Table 5 are more congruent with the notion of an average of the D−A distances reflecting fluctuations of the linker chains, intermediate in most cases between extended and folded conformational minima. Apparently the molecular geometries of closest D−A approach (columns 2−7) are not required to be the molecular conformations at which the energy transfer events take place.

CONCLUSIONS

We have elucidated excited state dynamics and photophysical properties of several related multichromophore triad systems based on pyrene and a short oligo-phenylenevinylene, exemplifying a "cable polymer" general design strategy for new optoelectronic materials. Time-resolved up-conversion measurements and steady state emission give details of the photoinduced energy transfer processes in the triads. Nonradiative energy transfer takes place from the S_1 excited state of the pyrene unit to the S_1 excited state of the *oligo*-phenylenevinylene core after excitation of the system with 265 nm pulses in a time scale of tens of picoseconds with k_{ET} = 1.1×10^{10} to 2.7×10^{10} s^{-1}.

The present studies determined directly the different energy transfer rate constants for each multichromophoric system. We can conclude that the energy transfer process is influenced not directly by linker length but by availability of molecular conformations with their respective fluctuations and rotations that allow the best approach of the donor and acceptor chromophores. This comes from comparisons of the time scales of rotational diffusion, determined from anisotropy measurements and comparisons with modeled conformational minima. Furthermore, we can conclude that some subset of excited state conformations favor the energy transfer process during the relaxation of the S_1 state of the triads, but apparently neither fully extended nor highly folded conformations is generally preferred. Finally, this work demonstrates that the linkage of pyrene units to an *oligo*-phenylenevinylene core using nonconjugated tethers with a length of eight atoms, as in the case of compounds **2**, **3**, and **5**, seems to give optimal effective energy transfer behavior, with transfer efficiencies of 87−96%.

dx.doi.org/10.1021/jp208602q | J. Phys. Chem. B 2012, 116, 3490−3503

■ ASSOCIATED CONTENT

Supporting Information

Additional figures and tables and complete references for refs 52 and 55. This material is available free of charge via the Internet at http://pubs.acs.org.

■ AUTHOR INFORMATION

Corresponding Author

*E-mail: jpeon@unam.mx.

Notes

The authors declare no competing financial interest.

■ ACKNOWLEDGMENTS

We are thankful to Professor Ahmed H. Zewail and the California Institute of Technology for the donation of equipment used in this study. For financial support, we are thankful to Consejo Nacional de Ciencia y Tecnología (CONACyT, Grant 79494) and to Universidad Nacional Autónoma de México (PAPIIT, Grant IN212907). We thank DGTIC-UNAM for some of the computational resources.

■ REFERENCES

(1) Nocera, D. G. *Inorg. Chem.* **2009**, *48*, 10001.
(2) Wasielewski, M. R. *Acc. Chem. Res.* **2009**, *42*, 1910.
(3) Kaletas, B. K.; Dobrawa, R.; Sautter, A.; Wuerthner, F.; Zimine, M.; De Cola, L.; Williams, R. M. *J. Phys. Chem. A* **2004**, *108*, 1900.
(4) Sierra, C. A.; Lahti, P. M. *J. Phys. Chem. A* **2006**, *110*, 12081.
(5) Sautter, A.; Kaletas, B. K.; Schmid, D. G.; Dobrawa, R.; Zimine, M.; Jung, G.; Van Stokkum, I. H. M.; De Cola, L.; Williams, R. M.; Wuerthner, F. *J. Am. Chem. Soc.* **2005**, *127*, 6719.
(6) Carmieli, R.; Mi, Q.; Butler Ricks, A.; Giacobbe, E. M.; Mickley, S. M.; Wasielewski, M. R. *J. Am. Chem. Soc.* **2009**, *131*, 8372.
(7) Gust, D.; Moore, T. A. *Science* **1989**, *244*, 35.
(8) Gust, D.; Moore, T. A.; Moore, A. L. *Acc. Chem. Res.* **1993**, *26*, 198.
(9) Gust, D.; Moore, T. A.; Moore, A. L.; Lee, S. J.; Bittersmann, E.; Luttrull, D. K.; Rehms, A. A.; DeGraziano, J. M.; Ma, X. C.; et al. *Science* **1990**, *248*, 199.
(10) Wasielewski, M. R. *Chem. Rev.* **1992**, *92*, 435.
(11) Tomizaki, K.; Loewe, R. S.; Kirmaier, C.; Schwartz, J. K.; Retsek, J. L.; Bocian, D. F.; Holten, D.; Lindsey, J. S. *J. Org. Chem.* **2002**, *67*, 6519.
(12) Cirpan, A.; Rathnayake, H. P.; Gunbas, G.; Lahti, P. M.; Karasz, F. E. *Synth. Met.* **2006**, *156*, 282.
(13) Cirpan, A.; Rathnayake, H. P.; Lahti, P. M.; Karasz, F. E. *J. Mater. Chem.* **2007**, *17*, 3030.
(14) Gurge, R. M.; Sarker, A.; Lahti, P. M.; Hu, B.; Karasz, F. E. *Macromolecules* **1996**, *29*, 4287.
(15) Gurge, R. M.; Sarker, A. M.; Lahti, P. M.; Hu, B.; Karasz, F. E. *Macromolecules* **1997**, *30*, 8286.
(16) Lahti, P. M.; Sarker, A.; Garay, R. O.; Lenz, R. W.; Karasz, F. E. *Polymer* **1994**, *35*, 1312.
(17) Liu, Y.; Lahti, P. M.; La, F. *Polymer* **1998**, *39*, 5241.
(18) Candeias, L. P.; Wildeman, J.; Hadziioannou, G.; Warman, J. M. *J. Phys. Chem. B* **2000**, *104*, 8366.
(19) Candeias, L. P.; Padmanaban, G.; Ramakrishnan, S. *Chem. Phys. Lett.* **2001**, *349*, 394.
(20) Seixas de Melo, J.; Pina, J.; Burrows, H. D.; Brocke, S.; Herzog, O.; Thorn-Csanyi, E. *Chem. Phys. Lett.* **2004**, *388*, 236.
(21) Bredas, J.-L.; Beljonne, D.; Coropceanu, V.; Cornil, J. *Chem. Rev.* **2004**, *104*, 4971.
(22) Seixas de Melo, J.; Pina, J.; Burrows, H. D.; Di Paolo, R. E.; Macanita, A. L. *Chem. Phys.* **2006**, *330*, 449.
(23) Di Paolo, R. E.; Seixas de Melo, J.; Pina, J.; Burrows, H. D.; Morgado, J.; Macanita, A. L. *ChemPhysChem* **2007**, *8*, 2657.
(24) Sluch, M. I.; Godt, A.; Bunz, U. H. F.; Berg, M. A. *J. Am. Chem. Soc.* **2001**, *123*, 6447.
(25) Collison, C. J.; Rothberg, L. J.; Treemaneekarn, V.; Li, Y. *Macromolecules* **2001**, *34*, 2346.
(26) Beljonne, D.; Shuai, Z.; Cornil, J.; Calbert, J. P.; Bredas, J. L. *J. Photochem. Photobiol., A* **2001**, *144*, 57.
(27) Dogariu, A.; Vacar, D.; Heeger, A. J. *Phys. Rev. B: Condens. Matter Mater. Phys.* **1998**, *58*, 10218.
(28) Hayes, G. R.; Samuel, I. D. W.; Phillips, R. T. *Phys. Rev. B: Condens. Matter Mater. Phys.* **1996**, *54*, R8301.
(29) Monkman, A. P.; Burrows, H. D.; Hamblett, I.; Navaratnam, S.; Scherf, U.; Schmitt, C. *Chem. Phys. Lett.* **2000**, *327*, 111.
(30) Monkman, A. P.; Burrows, H. D.; Miguel, M. D. G.; Hamblett, I.; Navaratnam, S. *Chem. Phys. Lett.* **1999**, *307*, 303.
(31) Foggi, P.; Pettini, L.; Santa, I.; Righini, R.; Califano, S. *J. Phys. Chem.* **1995**, *99*, 7439.
(32) Gritsan, N. P.; Pritchina, E. A.; Barabanov, I. I.; Burdzinski, G. T.; Platz, M. S. *J. Phys. Chem. C* **2009**, *113*, 11579.
(33) Raytchev, M.; Pandurski, E.; Buchvarov, I.; Modrakowski, C.; Fiebig, T. *J. Phys. Chem. A* **2003**, *107*, 4592.
(34) Abdel-Shafi, A. A.; Wilkinson, F. *J. Phys. Chem. A* **2000**, *104*, 5747.
(35) Craig, B. B.; Kirk, J.; Rodgers, M. A. J. *Chem. Phys. Lett.* **1977**, *49*, 437.
(36) Murov, S.; Carmichael, I.; Hug, G. L. In *Handbook of Photochemistry*, 2nd ed.; Marcel Dekker: New York, 1993.
(37) Devadoss, C.; Bharathi, P.; Moore, J. S. *J. Am. Chem. Soc.* **1996**, *118*, 9635.
(38) Friend, R. H.; Gymer, R. W.; Holmes, A. B.; Burroughes, J. H.; Marks, R. N.; Taliani, C.; Bradley, D. D. C.; Dos Santos, D. A.; Bredas, J. L.; Logdlund, M.; Salaneck, W. R. *Nature (London)* **1999**, *397*, 121.
(39) Campos, L. M.; Tontcheva, A.; Guenes, S.; Sonmez, G.; Neugebauer, H.; Sariciftci, N. S.; Wudl, F. *Chem. Mater.* **2005**, *17*, 4031.
(40) Guenes, S.; Neugebauer, H.; Sariciftci, N. S. *Chem. Rev.* **2007**, *107*, 1324.
(41) Kraabel, B.; Hummelen, J. C.; Vacar, D.; Moses, D.; Sariciftci, N. S.; Heeger, A. J.; Wudl, F. *J. Chem. Phys.* **1996**, *104*, 4267.
(42) Mozer, A. J.; Denk, P.; Scharber, M. C.; Neugebauer, H.; Sariciftci, N. S.; Wagner, P.; Lutsen, L.; Vanderzande, D. *J. Phys. Chem. B* **2004**, *108*, 5235.
(43) Kumar, N. D.; Lal, M.; Prasad, P. N. *Sci. Technol. Polym. Adv. Mater. [Proc. Int. Conf. Front. Polym. Adv. Mater.], 4th* 1998, 393.
(44) Yu, L.; Lin, G.; Liang, Y.; Yuan, S.; Lee, Y. *PMSE Prepr.* **2007**, *96*, 232.
(45) Thompson, B. C.; Frechet, J. M. J. *Angew. Chem., Int. Ed.* **2008**, *47*, 58.
(46) Rodriguez-Cordoba, W.; Zugazagoitia, J. S.; Collado-Fregoso, E.; Peon, J. *J. Phys. Chem. A* **2007**, *111*, 6241.
(47) Drexhage, K. H.; Erikson, G. R.; Hawks, G. H.; Reynolds, G. A. *Opt. Commun.* **1975**, *15*, 399.
(48) Allinger, N. L. *J. Am. Chem. Soc.* **1977**, *99*, 8127.
(49) Weiner, S. J.; Kollman, P. A.; Case, D. A.; Singh, U. C.; Ghio, C.; Alagona, G.; Profeta, S.; Weiner, P. *J. Am. Chem. Soc.* **1984**, *106*, 765.
(50) Cornell, W. D.; Cieplak, P.; Bayly, C. I.; Gould, I. R.; Merz, K. M.; Ferguson, D. M.; Spellmeyer, D. C.; Fox, T.; Caldwell, J. W.; Kollman, P. A. *J. Am. Chem. Soc.* **1995**, *117*, 5179.
(51) Smith, J. C.; Karplus, M. *J. Am. Chem. Soc.* **1992**, *114*, 801.
(52) MacKerell, A. D.; Bashford, D.; Bellott; Dunbrack, R. L.; Evanseck, J. D.; Field, M. J.; Fischer, S.; Gao, J.; Guo, H.; Ha, S.; et al. *J. Phys. Chem. B* **1998**, *102*, 3586.
(53) HyperChem(TM), H., Inc., 1115 NW 4th Street, Gainesville, FL 32601, USA.
(54) Rappe, A. K.; Casewit, C. J.; Colwell, K. S.; Goddard, W. A.; Skiff, W. M. *J. Am. Chem. Soc.* **1992**, *114*, 10024.
(55) Frisch, M. J.; Trucks, G. W.; Schlegel, H. B.; Scuseria, G. E.; Robb, M. A.; Cheeseman, J. R.; Scalmani, G.; Barone, V.; Mennucci, B.; Petersson, G. A.; et al. *Gaussian 09*; Gaussian, Inc.: Wallingford, CT, 2009.

(56) Becke, A. D. *J. Chem. Phys.* **1993**, *98*, 5648.
(57) Narwark, O.; Gerhard, A.; Meskers, S. C. J.; Brocke, S.; Thorn-Csanyi, E.; Bassler, H. *Chem. Phys.* **2003**, *294*, 17.
(58) Narwark, O.; Meskers, S. C. J.; Peetz, R.; Thorn-Csanyi, E.; Bassler, H. *Chem. Phys.* **2003**, *294*, 1.
(59) Speiser, S. *Chem. Rev.* **1996**, *96*, 1953.
(60) Förster, T. *Ann. Phys. (Leipzig)* **1948**, *2*, 55.
(61) Förster, T. *Z. Naturforsch.* **1949**, *4a*, 321.
(62) Förster, T. *Discuss. Faraday Soc.* **1959**, *27*, 7.
(63) Chang, R.; Hsu, J. H.; Fann, W. S.; Liang, K. K.; Chang, C. H.; Hayashi, M.; Yu, J.; Lin, S. H.; Chang, E. C.; Chuang, K. R.; Chen, S. A. *Chem. Phys. Lett.* **2000**, *317*, 142.
(64) Gierschner, J.; Mack, H.-G.; Luer, L.; Oelkrug, D. *J. Chem. Phys.* **2002**, *116*, 8596.
(65) Grage, M. M. L.; Wood, P. W.; Ruseckas, A.; Pullerits, T.; Mitchell, W.; Burn, P. L.; Samuel, I. D. W.; Sundstrom, V. *J. Chem. Phys.* **2003**, *118*, 7644.
(66) Li, N.; Jia, K.; Wang, S.; Xia, A. *J. Phys. Chem. A* **2007**, *111*, 9393.
(67) Nguyen, T.-Q.; Doan, V.; Schwartz, B. J. *J. Chem. Phys.* **1999**, *110*, 4068.
(68) Yang, H.-C.; Hua, C.-Y.; Kuo, M.-Y.; Huang, Q.; Chen, C.-L. *ChemPhysChem* **2004**, *5*, 373.
(69) Zhang, H.; Lu, X.; Li, Y.; Ai, X.; Zhang, X.; Yang, G. *J. Photochem. Photobiol., A* **2002**, *147*, 15.
(70) Kozyra, K. A.; Heldt, J. R.; Heldt, J.; Engelke, M.; Diehl, H. A. *Z. Naturforsch., A: Phys. Sci.* **2003**, *58*, 581.
(71) Jozefowicz, M.; Heldt, J. R.; Bajorek, A.; Paczkowski, J. *J. Photochem. Photobiol., A* **2008**, *196*, 38.
(72) van, V. E.; Zhang, H.; Glasbeek, M. *J. Phys. Chem. A* **2001**, *105*, 1687.
(73) Horng, M. L.; Gardecki, J. A.; Papazyan, A.; Maroncelli, M. *J. Phys. Chem.* **1995**, *99*, 17311.
(74) Karpovich, D. S.; Blanchard, G. J. *J. Phys. Chem.* **1995**, *99*, 3951.